The Role of Driving Energy and Delocalized States for Charge Separation in Organic Semiconductors

Bakulin, Artem A.; Rao, Akshay; Pavelyev, Vlad G.; van Loosdrecht, Paul H. M.; Pshenichnikov, Maxim S.; Niedzialek, Dorota; Cornil, Jerome; Beljonne, David; Friend, Richard H.; Cornil, Jérôme

Published in:
Science

DOI:
10.1126/science.1217745

Publication date:
2012

www.sciencemag.org/cgi/content/full/science.1217745/DC1

Supporting Online Material for

The Role of Driving Energy and Delocalized States for Charge Separation in Organic Semiconductors

Artem A. Bakulin, Akshay Rao, Vlad G. Pavelyev, Paul H. M. van Loosdrecht, Maxim S. Pshenichnikov, Dorota Niedzialek, Jérôme Cornil, David Beljonne, Richard H. Friend*

*To whom correspondence should be addressed. E-mail: rhf10@cam.ac.uk

Published 23 February 2012 on *Science* Express
DOI: 10.1126/science.1217745

This PDF file includes:

1. Materials and Methods

Materials: PFB, F8BT, F8TBT were provided by Cambridge Display Technologies, MDMO-PPV and P3HT were purchased from Merck, $PC_{70}BM$ from NanoC, PCDTBT and PCPDTBT from One-materials.

Films preparation: Spectrosil fused silica substrates were first cleaned by sonication in acetone and isopropanol. 1:2 blend of PCPDTBT:$PC_{70}BM$ (30mg/ml in chlorobenzene with 5% 1,8-octanedithiol), 1:4 blends of PCDTBT:$PC_{70}BM$ (30mg/ml in dichlorobenzene) and 1:4 blend of MDMO-PPV:$PC_{70}BM$ (15mg/ml in chlorobenzene) were spun on cleaned substrates in a nitrogen filled glovebox. PCDTBT:$PC_{70}BM$ and PCPDTBT:$PC_{70}BM$ samples were allowed to dry for 30 minutes at 70°C.

Device preparation: Indium-tin-oxide-coated (ITO) glass substrates were cleaned by sonication in acetone and isopropanol, followed by oxygen plasma treatment. A 40 nm thick PEDOT:PSS layer was deposited onto the plasma-treated substrates and then annealed at 230°C for 30 minutes under flowing nitrogen. The substrates were then transferred into a nitrogen glovebox for the further fabrication steps. 1:2 blend of PCPDTBT:$PC_{70}BM$ (30mg/ml in chlorobenzene with 5% 1,8-octanedithiol), 1:4 blends of PCDTBT:$PC_{70}BM$ (30mg/ml in dichlorobenzene) and 1:4 blend of MDMO-PPV:$PC_{70}BM$ (15mg/ml in chlorobenzene), 1:1 blend of P3HT:$PC_{60}BM$ (30mg/ml in dichlorobenzene), 1:1 blend of P3HT:F8TBT (20mg/ml in xylene) and 1:1 blend of PFB:F8BT (20mg/ml in chloroform) were then spun on cleaned and plasma treated ITO substrates. PCDTBT:$PC_{70}BM$ and PCPDTBT:$PC_{70}BM$ samples were allowed to dry for 30 minutes at 70°C. P3HT:$PC_{60}BM$ samples were annealed at 140°C for 10min. Samples were then transferred to a thermal evaporator within the glovebox where 120nm thick Al electrodes were deposited under a vacuum better than 10^{-6} mbar. P3HT:F8TBT samples were then post annealed at 140°C. All samples were encapsulated before testing.

Pump-Push Photocurrent experiments: (fig 2D, main text) were performed using commercial regenerative 1kHz Ti:Sapphire amplifier (Spectra Physics, Solstice) pumping home-build broadband NOPA used for generating pump and commercial OPA (Light Conversion, TOPAS) to generate the push pulse (2200nm, ~1 μJ). Reference photocurrent from photodiode was detected on pump repetition frequency of 1 kHz by a lock-in amplifier. The push beam was mechanically chopped at 500 Hz and its effect on the photocurrent was also detected by a lock-in technique. For simultaneous measurement of photoinduced absorption push beam was detected by the photodiode and used as a probe.

Push pulse energy needed for a good signal-to-noise was as high as ~1 μJ (~3mJ/cm^2). To avoid experimental artefacts we measured the intensity dependence of the signal. For some of samples multiphoton contributions to the signal were observed at higher push energies of 5-10 μJ (~30 mJ/cm^2). To avoid multiphoton absorption, the push pulse energy was lowered until the linear dependence on the push intensity was reached.

3-pulse experiments: (fig 2E, main text) were performed using setup described in Ref. (*44*). A home-built Ti:Sapphire amplifier was used to pump a non-collinear optical parametrical amplifier (NOPA), providing pump pulses (500-700 nm, 30 fs, <0.1 μJ per pulse), and an optical parametric amplifier (OPA), generating the IR push and probe (*45*). Although the pump pulse was relatively intense the low extinction of the sample at the absorption edge provided low spatial density of states homogeneously redistributed in the film. The ~1 μJ push and 5 nJ probe pulses having duration of ~70 fs and a bandwidth of ~300 nm FWHM, were positioned at 3300 nm. The polarizations of the IR-push was rotated by 54.7^{o} (magic angle) with respect to the polarization of the pump beam. After the sample, the probe components of different polarisation were detected by InSb photodiodes. All data were obtained at 300 K. During the measurements the pump beam was mechanically modulated at 500 Hz rate and push beam at 250 Hz rate, both rates being phase-locked to the laser 1kHz repetition frequency. The pump, push, probes (parallel and perpendicular components), and probe-reference intensities was simultaneously detected and digitized using an ADC card. This approach allowed simultaneous detection of charge dynamics with and without push pulse at high frequency and therefore with minimal noise.

2. Details of charge-transfer state modeling

In the first series of calculations, we explore the amount of charge delocalization upon IR absorption in single conjugated polymer chains. These calculations are performed at the AM1/SCI (*46*) level and aim at calculating the positive polaron absorption in P3HT and MDMO-PPV chains containing 10 repeat units. For the sake of simplicity, the long alkyl chains were replaced with methyl groups. The geometry has been optimized in the singly positively charged state without any constraint of planarity. The results reported below have been obtained using an active space of 100 active molecular orbitals using the 9.1 version of the Ampac package (*47*). The lowest polaron absorption, calculated at about 0.8eV in both systems (Figure S1), involves namely electronic transitions from the delocalized valence orbitals to the SOMO 'π' orbital confined around the central part of the chains. Compared to the charged ground state, the resulting excited state features a more delocalized charge distribution, as can be seen from Figure S2. We stress that this effect has primarily an electronic origin, yet the more confined charged distribution in the ground state is reinforced upon geometric relaxation (*i.e.*, polaron formation).

It is important to note here that in contrast to the ground polaron state CT_0 the distributions of charge in the excited polaron states CT_n are very similar for different chain geometries and bringing polaron to the excited state can dramatically decrease the coupling to the environment. This was analytically highlighted before by Brazovskii and Kirova (*19*), who showed that the presence of the polaron distortion leaves all other π band states unchanged. This is confirmed by the results of our calculation presented in figure S3. While in the ground state charge is much more localised after geometrical relaxation of the chain, charge distribution in the polaron excited state is very similar for

both geometries. This confirms that the push-induced states investigated in the experiment are very similar to those populated directly after exciton-dissociation.

In a second part of the modeling work, we first assess the geometry of polymer-PCBM and polymer-polymer heterojunctions using force-field techniques. MD simulations (100ps, NVT ensemble) are performed using the COMPASS force field (*48*) followed by full geometry optimization at 0K. The electronic excited states are then calculated at the INDO (*49*)/SCI level (active space of 100 occupied and 100 unoccupied molecular orbitals) in presence of a static electric field (to mimic the environment). The field is adjusted in order to stabilize and isolate the charge-transfer state as the lowest electronic excited state (energy offset with respect to the lowest localized excited state of -0.5eV for P3HT/PCBM and -0.3eV for P3HT/F8TBT). While the value of the electron-hole radius is sensitive to the choice of the electric field, the overall picture, namely the increased charge separation in the higher-lying CT* excited state, remains unchanged.

Figures S4 and S5 show the changes in the charge density distribution upon going from the neutral ground state to the lowest CT state as well as from CT to the strongly dipole coupled CT* excited state in P3HT/PCBM. The INDO/SCI simulated optical absorption from the CT state is shown on Figure S6. The corresponding results for P3HT/F8TBT are given in Figures S7-S9. The results obtained on the donor-acceptor pairs confirm the more delocalized character of the hole wavefunction in the charge-transfer excited state reached upon transient absorption of the IR push. The larger delocalization along the donor polymer chain translates into a larger intermolecular electron-hole separation. Note that, in these calculations, the increased CT radius is entirely due to electron-hole correlation effects.

3. Typical conditions of pump-push experiment

In the pump-push photocurrent experiment the OPV device was irradiated with a visible (Vis) pump pulse, which was absorbed in the active layer and created a population of charges (CT) states with high quantum efficiency. After this, the sample was irradiated by an IR push pulse, which was selectively absorbed by created CT states. The pump-induced absorption of the push (dT/T) was detected in a parallel experiment with a photodiode.

Knowing the power of IR beam and IR photoinduced absorption we calculate the total number of IR-push photons absorbed. Then the number of Vis photons absorbed in the sample, and therefore peak concentration of CT states, is calculated using the energy of the visible pump pulse and the energy of a single photon. Assuming 100% efficient generation of charged states from Vis pump photons, we then calculate the number of absorbed IR photons per hole (bound or free). Then we normalize by this value the detected change in photocurrent (δPC/PC) to determine the relative change in photocurrent per IR photon per charge pair. This is the final value used in the discussion.

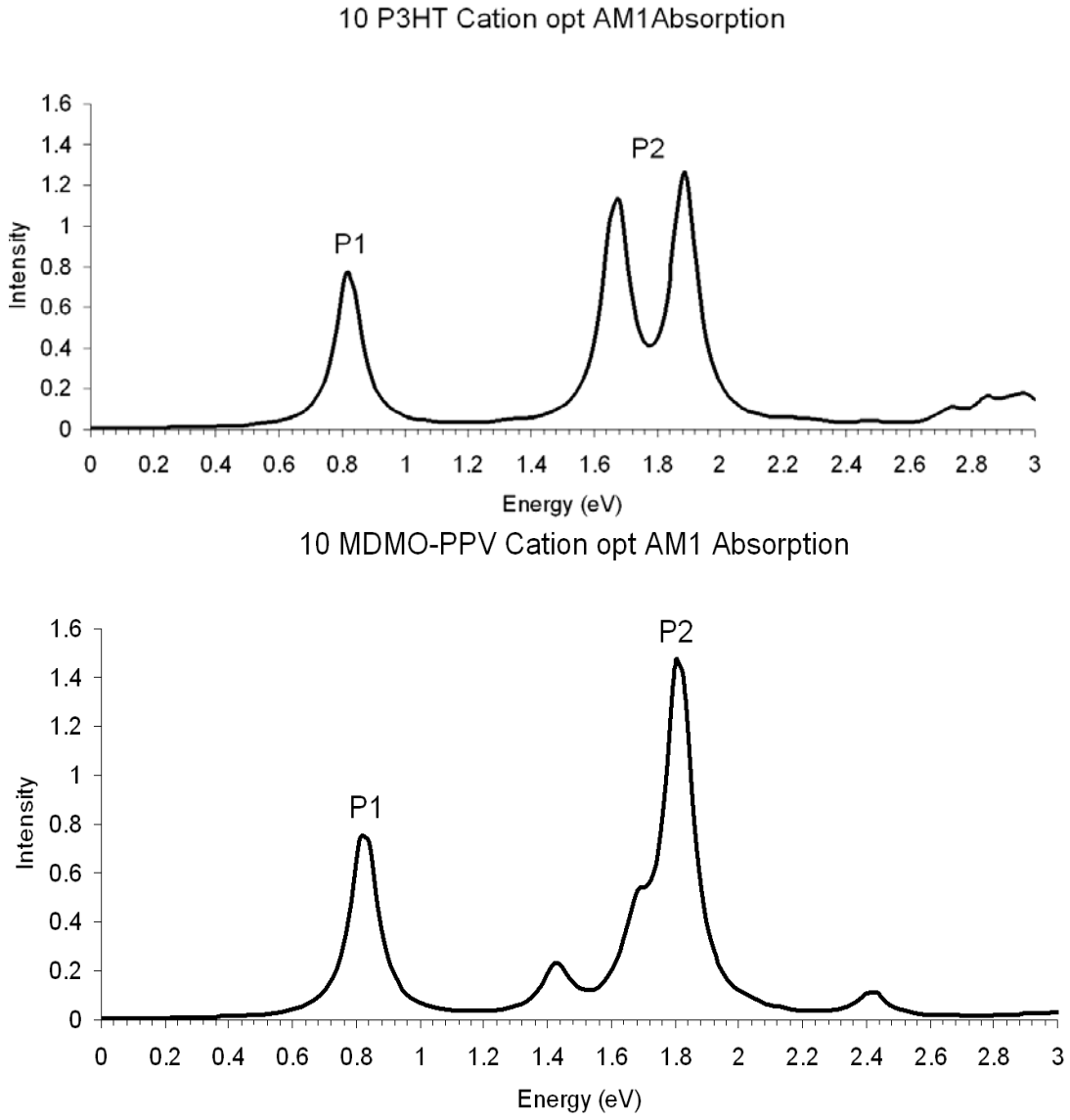

Figure S1: AM1/SCI simulated polaron absorption (from the relaxed geometry of the singly positively charged molecule) in P3HT (top) and MDMO-PPV (bottom) 10-mer chains. P1 involves electronic excitations from the delocalized valence levels to the localized π polaron state.

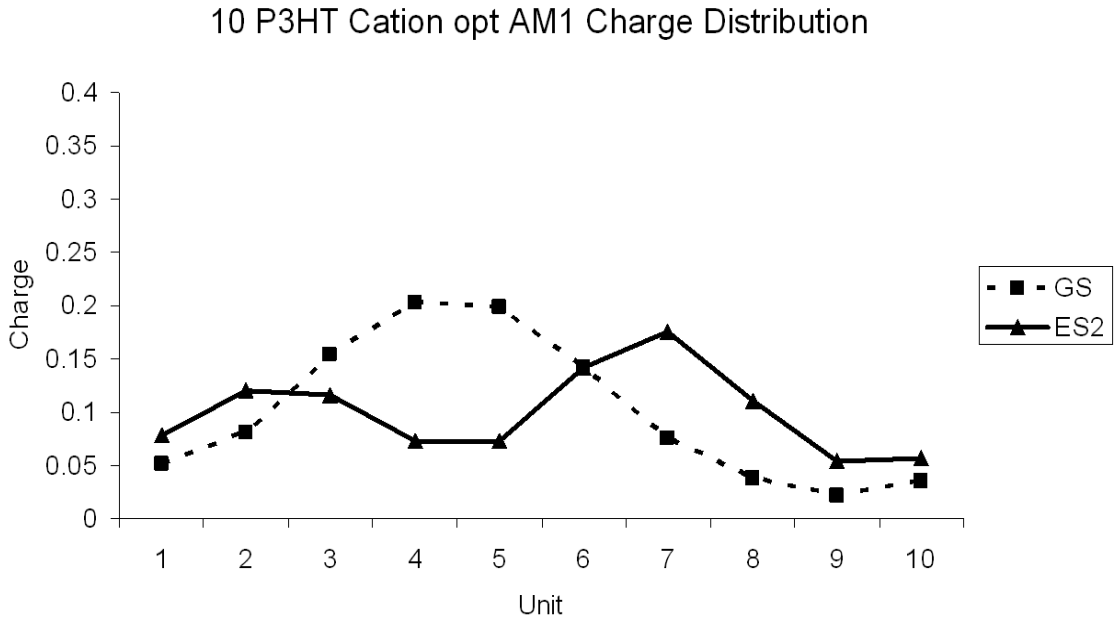
10 P3HT Cation opt AM1 Charge Distribution
Charge
0.4
0.35
0.3
0.25
0.2
0.15
0.1
0.05
0
1
2
3
4
5
6
7
8
9
10
Unit
GS
ES2

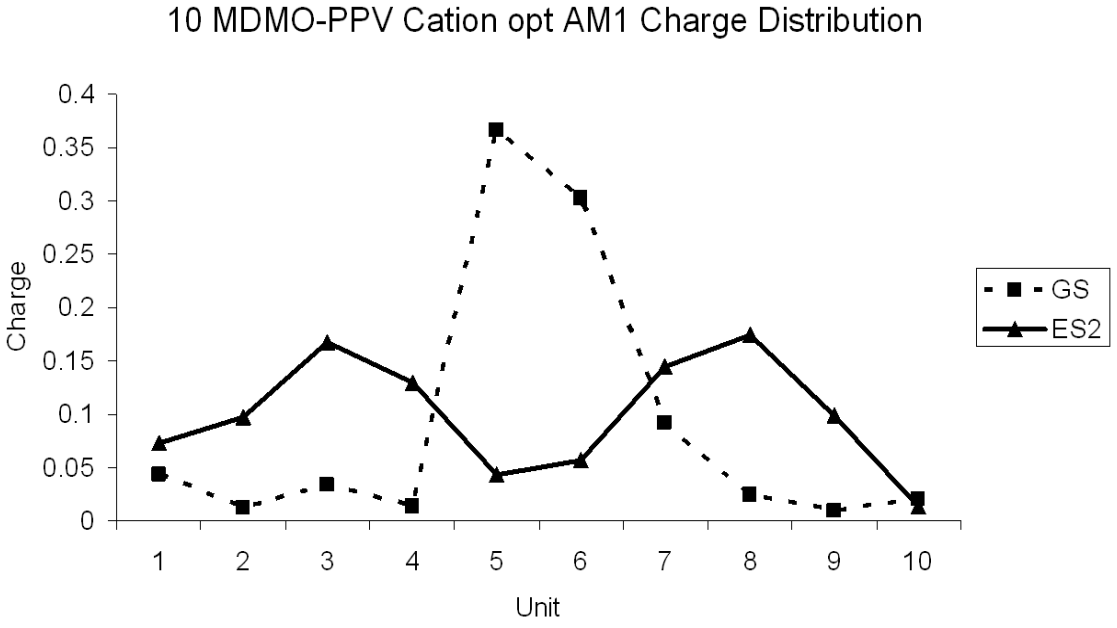
10 MDMO-PPV Cation opt AM1 Charge Distribution
Charge
0.4
0.35
0.3
0.25
0.2
0.15
0.1
0.05
0
1
2
3
4
5
6
7
8
9
10
Unit
GS
ES2

Figure S2: AM1/SCI calculated charge distribution per repeating unit based on a Mulliken population analysis in the charged ground state and in the P1 excited state in P3HT and MDMO-PPV 10-mer chains.

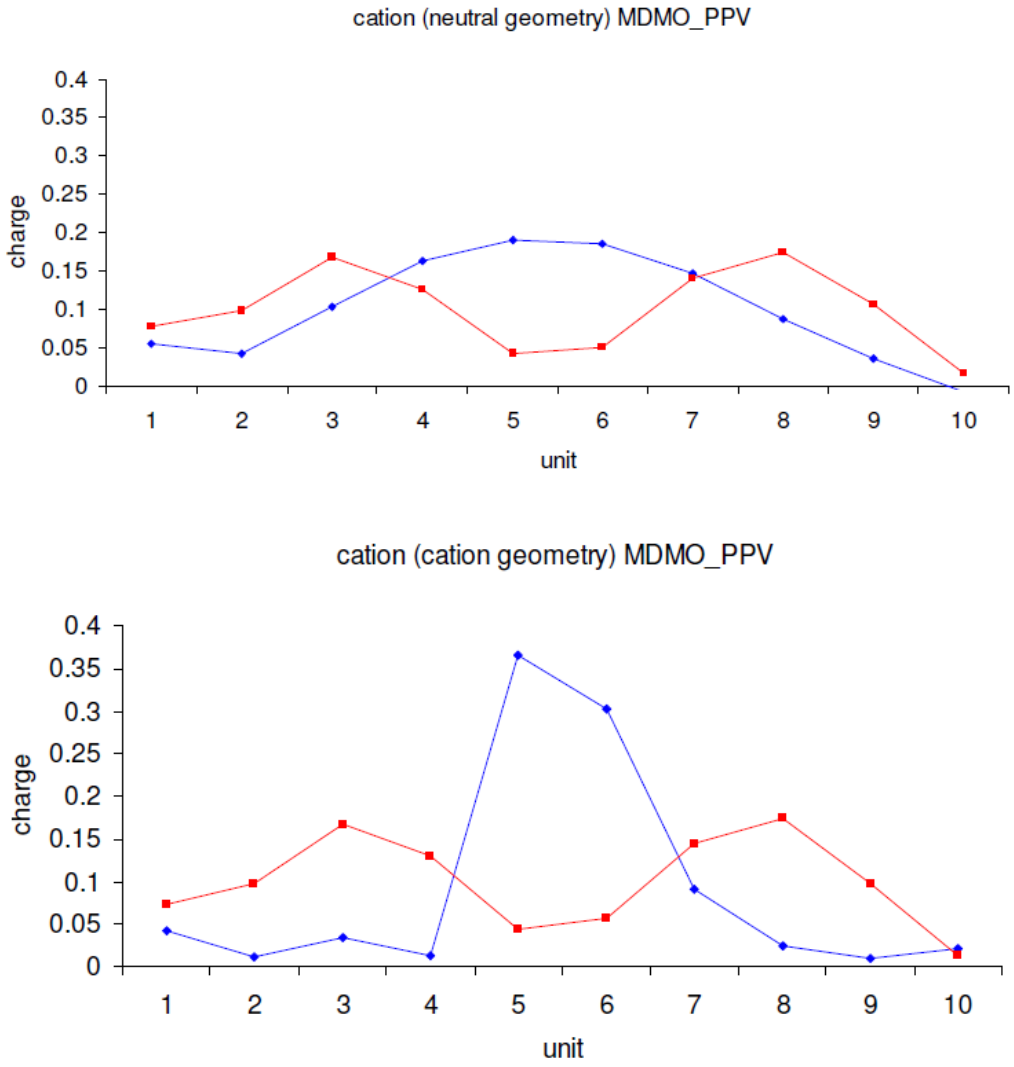

Figure S3: AM1/SCI calculated charge distribution per repeating unit based on a Mulliken population analysis in the charged ground state (blue) and in the P1 excited state (red) for MDMO-PPV 10-mer chain in neutral geometry (top) and after the polaronic geometrical relaxation (bottom).

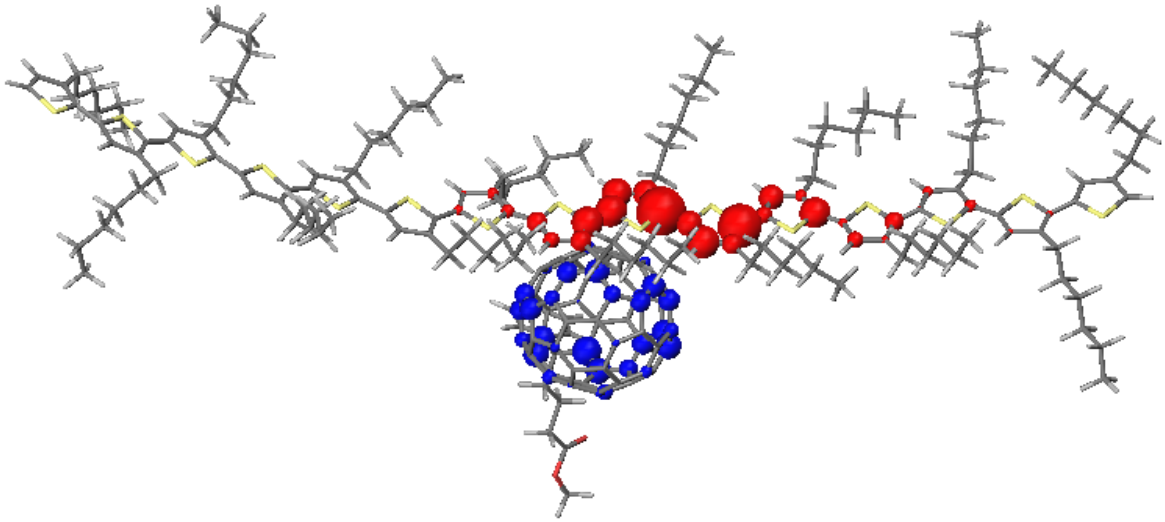

Figure S4: INDO/SCI charge density redistribution when going from the neutral ground state to the lowest charge-transfer state (CT). Red circles for positive partial charges, blue circles for negative partial charges. Note the rather confined electron-hole pair, which here simply results from electrostatics (no nuclear relaxation). Electron-hole radius: 9.8 Å.

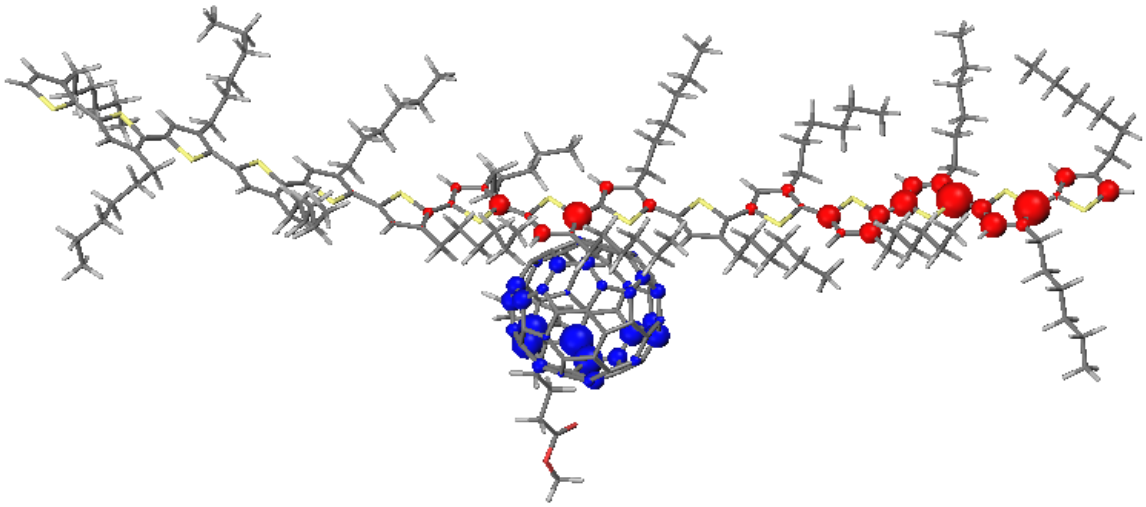

Figure S5: Same as Fig.S4 for the CT* excited state, strongly dipole coupled to CT. Note the more delocalized character of the hole. Electron-hole radius: 13.7Å.

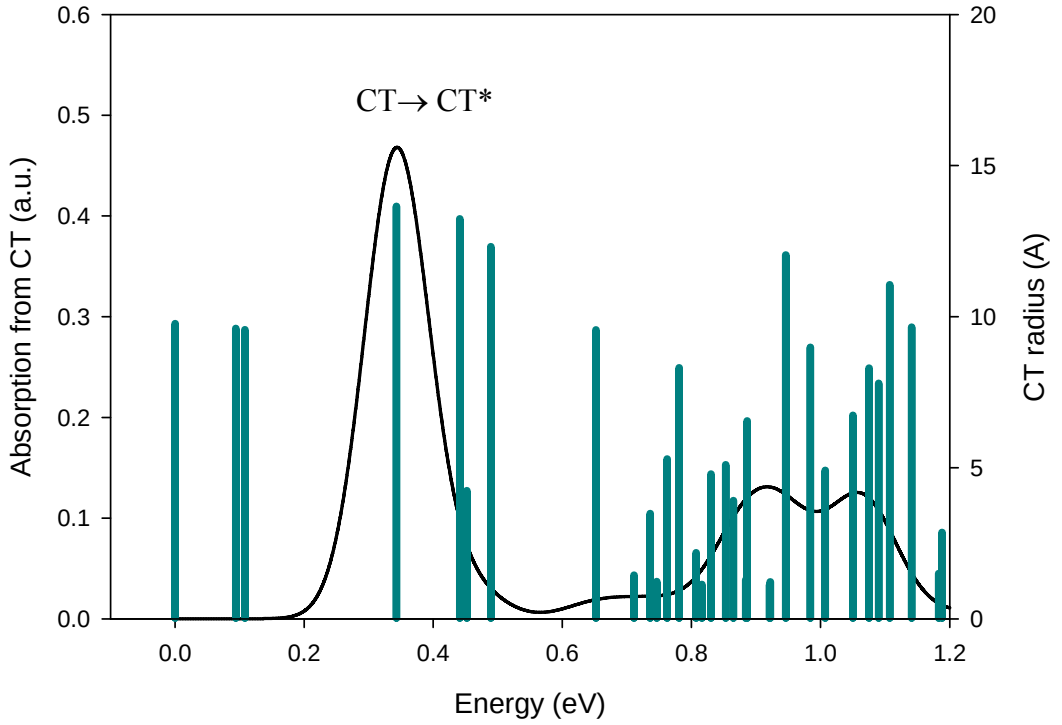

Figure S6: INDO/SCI simulated absorption spectrum from the lowest charge transfer state, CT, and intermolecular electron-hole radius in P3HT/PCBM. Note the increased electron-hole separation for the excited states CT*, dipole coupled to CT.

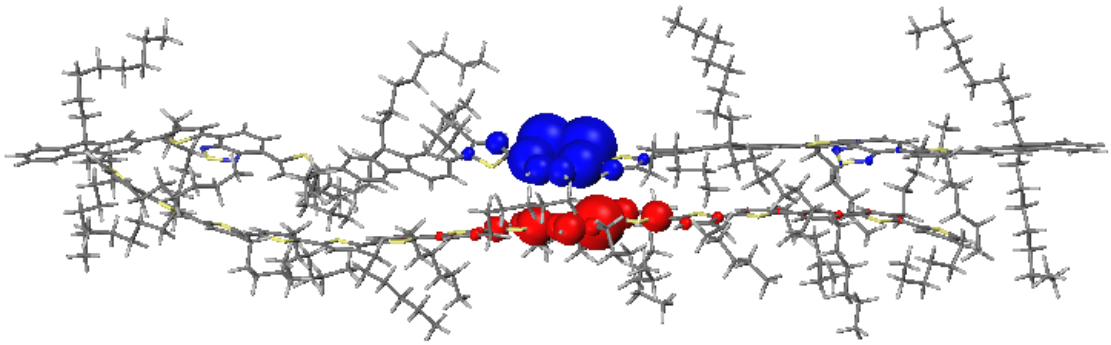

Figure S7: Charge density redistribution when going from the neutral ground state to the lowest charge transfer state, CT. Red circles for positive partial charges, blue circles for negative partial charges. Note the rather confined electron-hole pair, which here simply results from electrostatics (no nuclear relaxation). Electron-hole average intermolecular radius: 6.2Å. It is worth noting that this value is smaller than that obtained for the corresponding transition in P3HT/PCBM (which can be understood from a simple geometric point of view: larger center-to-center separation).

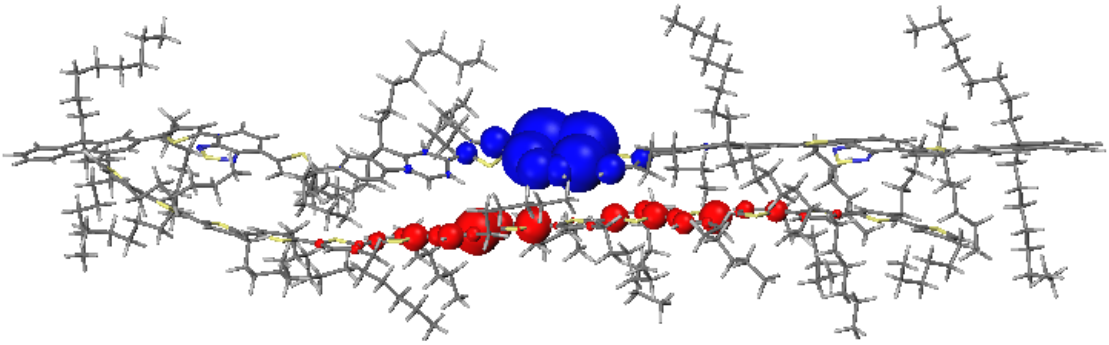

Figure S8: Same as Fig. S6 for the CT* excited state, strongly dipole coupled to CT. Note the more delocalized character of the hole. Electron-hole average intermolecular radius: 8.3Å

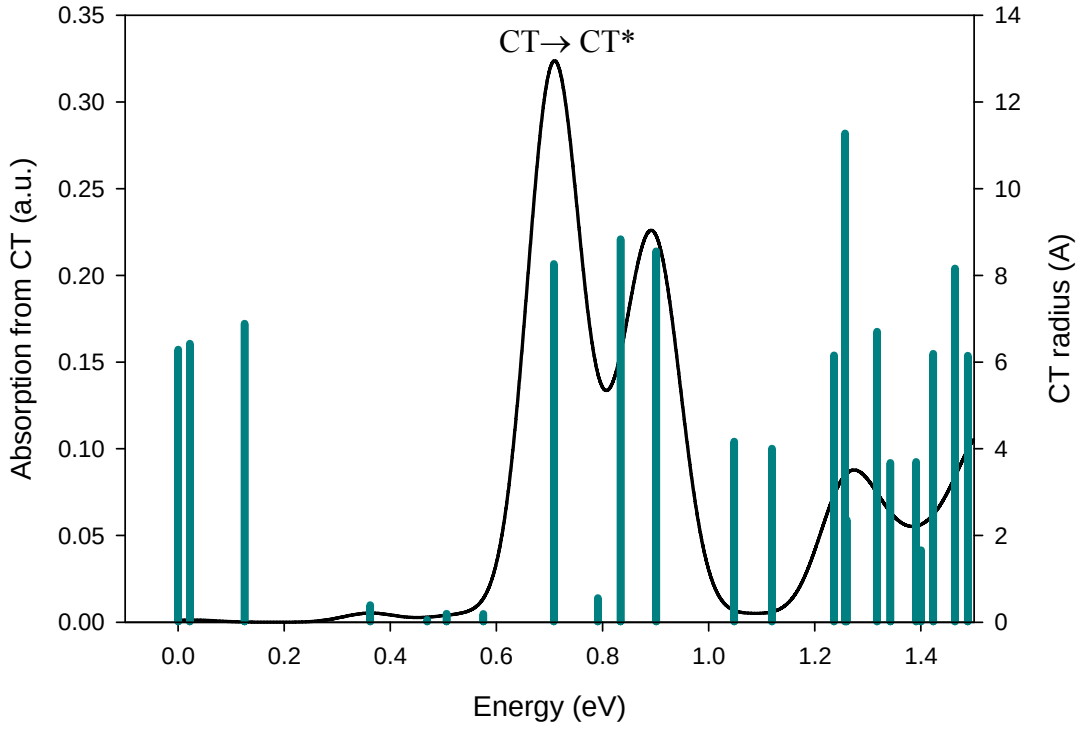

Figure S9: INDO/SCI simulated absorption spectrum from the lowest charge transfer state, CT, and intermolecular electron-hole radius in P3HT/F8TBT. Note the increased electron-hole separation for the excited states CT*, strongly dipole coupled to CT.

S10. Table summarizing typical conditions and recorded values in a set of pump-push experiments on OPV devices. Push pulse energy was 1 μJ for all the experiments.

Material	WL (nm)	Pump E (nJ)	max dPC/PC	dT/T @2.2um	Num. VIS pump photons	Num. IR push photons	IR photons per CT state	δPC/PC per IR per CT state
PFB:F8BT	540	12	1.00E-03	1.71E-05	3.85E+10	1.71E+08	4.46E-03	2.24E-01
P3HT:F8TBT	590	0.9	4.50E-04	1.25E-06	3.21E+09	1.25E+07	3.89E-03	1.16E-01
MDMO-PPV: PC70BM	590	1.2	1.40E-03	1.20E-05	3.81E+09	1.20E+08	3.15E-02	4.44E-02
P3HT:PCBM	590	0.4	1.40E-04	1.82E-06	1.29E+09	1.82E+07	1.41E-02	9.94E-03
PCPDTBT: PC70BM	680	0.8	2.40E-05	1.14E-06	2.92E+09	1.14E+07	3.91E-03	6.14E-03
PCDTBT: PC70BM	650	0.7	-3.00E-05	1.17E-06	2.45E+09	1.17E+07	4.77E-03	-6.29E-03

References and Notes

1. R. E. Blankenship, *Molecular Mechanisms of Photosynthesis*. (Blackwell Science, Oxford, 2002).
2. T. M. Clarke, J. R. Durrant, *Chem. Rev.* **110**, 6736 (2010).
3. G. Yu, J. Gao, J. C. Hummelen, F. Wudl, A. J. Heeger, *Science* **270**, 1789 (1995).
4. M. M. Wienk *et al*., *Angew. Chem. Int. Ed.* **42**, 3371 (2003).
5. Y. Kim *et al*., *Nat. Mater.* **5**, 197 (2006).
6. J. Peet *et al*., *Nat. Mater.* **6**, 497 (2007).
7. C. R. McNeill *et al*., *Adv. Funct. Mater.* **18**, 2309 (2008).
8. R.-Q. Png *et al*., *Nat. Mater.* **9**, 152 (2010).
9. S. H. Park *et al*., *Nat. Photonics* **3**, 297 (2009).
10. C. Deibel, T. Strobel, V. Dyakonov, *Adv. Mater.* **22**, 4097 (2010).
11. S. Shoaee *et al*., *J. Am. Chem. Soc.* **132**, 12919 (2010).

12. J.-L. Brédas, J. E. Norton, J. Cornil, V. Coropceanu, *Acc. Chem. Res.* **42**, 1691 (2009).

13. T. Strobel, C. Deibel, V. Dyakonov, *Phys. Rev. Lett.* **105**, 266602 (2010).

14. F. Etzold *et al*., *J. Am. Chem. Soc.* **133**, 9469 (2011).

15. S. Gélinas *et al*., *J. Phys. Chem. C* **115**, 7114 (2011).

16. A. C. Morteani, P. Sreearunothai, L. M. Herz, R. H. Friend, C. Silva, *Phys. Rev. Lett.* **92**, 247402 (2004).

17. M. R. Jones, *Biochem. Soc. Trans.* **37**, 400 (2009).

18. J. Piris *et al*., *J. Phys. Chem. C* **113**, 14500 (2009).

19. S. A. Brazovskii, N. N. Kirova, *JETP Lett.* **33**, 4 (1981).

20. D. K. Campbell, A. R. Bishop, K. Fesser, *Phys. Rev. B* **26**, 6862 (1982).

21. X. Wei, Z. V. Vardeny, N. S. Sariciftci, A. J. Heeger, *Phys. Rev. B* **53**, 2187 (1996).

22. R. Österbacka, C. P. An, X. M. Jiang, Z. V. Vardeny, *Science* **287**, 839 (2000).

23. K. Vandewal, K. Tvingstedt, A. Gadisa, O. Inganäs, J. V. Manca, *Nat. Mater.* **8**, 904 (2009).

24. J. G. Müller *et al*., *Phys. Rev. B* **72**, 195208 (2005).

25. J. G. Müller, U. Lemmer, J. Feldmann, U. Scherf, *Phys. Rev. Lett.* **88**, 147401 (2002).

26. S. V. Frolov, Z. Bao, M. Wohlgenannt, Z. V. Vardeny, *Phys. Rev. B* **65**, 205209 (2002).

27. Materials and methods are available as supporting material on *Science* Online.

28. M. A. Loi *et al*., *Adv. Funct. Mater.* **17**, 2111 (2007).

29. D. Veldman *et al*., *J. Am. Chem. Soc.* **130**, 7721 (2008).

30. R. D. Pensack, J. B. Asbury, *J. Am. Chem. Soc.* **131**, 15986 (2009).

31. J. Lee *et al*., *J. Am. Chem. Soc.* **132**, 11878 (2010).

32. V. I. Arkhipov, P. Heremans, H. Bassler, *Appl. Phys. Lett.* **82**, 4605 (2003).

33. D. Veldman, S. C. J. Meskers, R. A. J. Janssen, *Adv. Funct. Mater.* **19**, 1939 (2009).

34. A. A. Bakulin, D. Martyanov, D. Y. Paraschuk, P. H. M. van Loosdrecht, M. S. Pshenichnikov, *Chem. Phys. Lett.* **482**, 99 (2009).

35. R. A. Marsh, J. M. Hodgkiss, R. H. Friend, *Adv. Mater.* **22**, 3672 (2010).

36. J. J. Benson-Smith *et al*., *Adv. Funct. Mater.* **17**, 451 (2007).

37. K. Vandewal, K. Tvingstedt, A. Gadisa, O. Inganas, J. V. Manca, *Phys. Rev. B* **81**, 125204 (2010).

38. Y. S. Huang *et al*., *Nat. Mater.* **7**, 483 (2008).

39. J. Holt, S. Singh, T. Drori, Y. Zhang, Z. V. Vardeny, *Phys. Rev. B* **79**, 195210 (2009).

40. T. Drori, J. Holt, Z. V. Vardeny, *Phys. Rev. B* **82**, 075207 (2010).

41. G. D. Scholes, *ACS Nano* **2**, 523 (2008).

42. Y. Matsuo *et al*., *J. Am. Chem. Soc.* **131**, 16048 (2009).

43. R. F. Service, *Science* **332**, 293 (2011).

44. A. A. Bakulin, D. S. Martyanov, D. Y. Paraschuk, M. S. Pshenichnikov, P. H. M. van Loosdrecht, *J. Phys. Chem. B* **112**, 13730 (2008).

45. S. Yeremenko, A. Baltuska, F. de Haan, M. S. Pshenichnikov, D. A. Wiersma, *Opt. Lett.* **27**, 1171 (2002).

46. M. J. S. Dewar, E. G. Zoebisch, E. F. Healy, J. J. P. Stewart, *J. Am. Chem. Soc.* **107**, 3902 (1985).

47. http://www.semichem.com/ampac/

48. H. Sun, *J. Phys. Chem. B* **102**, 7338 (1998).

49. M. C. Zerner, G. H. Loew, R. F. Kirchner, U. T. Mueller-Westerhoff, *J. Am. Chem. Soc.* **102**, 589 (1980).